THE JOURNAL OF BIOLOGICAL CHEMISTRY VOL. 288, NO. 27, pp. 19796–19804, July 5, 2013

Insights into the Photoprotective Switch of the Major Light-harvesting Complex II (LHCII)

*A PRESERVED CORE OF ARGININE-GLUTAMATE INTERLOCKED HELICES COMPLEMENTED BY ADJUSTABLE LOOPS**

Received for publication, January 24, 2013, and in revised form, April 29, 2013 Published, JBC Papers in Press, April 29, 2013, DOI 10.1074/jbc.M113.456111

Kiran Sunku[‡], Huub. J. M. de Groot[‡], and Anjali Pandit[§1]

From the [‡]Department of Solid-State NMR, Leiden Institute of Chemistry, Gorlaeus Laboratory, Leiden University, Einsteinweg 55, 2300 RA Leiden and the [§]Biophysics Group, Department of Physics and Astronomy, Faculty of Sciences, Vrije Universiteit, De Boelelaan 1081, 1081 HV Amsterdam, The Netherlands

Background: The peripheral light-harvesting complexes of photosystem II (LHCII) switch between light energy capturing and dissipative states.
Results: An NMR analysis is presented of the arginines in LHCII prepared in its two states.
Conclusion: The protein core of arginine-glutamate interlocked helices is preserved, whereas moderate changes occur in the stromal loop region.
Significance: This work reveals consequences for the molecular switching of LHCII.

Light-harvesting antennae of the LHC family form transmembrane three-helix bundles of which two helices are interlocked by conserved arginine-glutamate (Arg-Glu) ion pairs that form ligation sites for chlorophylls. The antenna proteins of photosystem II have an intriguing dual function. In excess light, they can switch their conformation from a light-harvesting into a photoprotective state, in which the excess and harmful excitation energies are safely dissipated as heat. Here we applied magic angle spinning NMR and selective Arg isotope enrichment as a noninvasive method to analyze the Arg structures of the major light-harvesting complex II (LHCII). The conformations of the Arg residues that interlock helix A and B appear to be preserved in the light-harvesting and photoprotective state. Several Arg residues have very downfield-shifted proton NMR responses, indicating that they stabilize the complex by strong hydrogen bonds. For the Arg C_α chemical shifts, differences are observed between LHCII in the active, light-harvesting and in the photoprotective, quenched state. These differences are attributed to a conformational change of the Arg residue in the stromal loop region. We conclude that the interlocked helices of LHCII form a rigid core. Consequently, the LHCII conformational switch does not involve changes in A/B helix tilting but likely involves rearrangements of the loops and helical segments close to the stromal and lumenal ends.

The elementary step in photosynthesis is the capture of solar energy by the light-harvesting antenna. In eukaryotic organisms, this step is performed by a family of pigment-binding proteins called light-harvesting complexes (LHCs)[2] that absorb sunlight and transfer the excitation energy toward the reaction centers, where charge separation takes place (1). The Lhcb antenna proteins of higher plants and moss and Lhcbm antenna proteins of LHCs in green algae contain three membrane-spanning helices A, B, and C, and their tertiary structure is typified by two crossing A/B helices interconnected by Arg-Glu ion pairs that form ligation sites for Chls.

The most abundant LHC in plants and green algae is the major light-harvesting complex II (LHCII), which captures about 50% of all land-bound chlorophylls. The LHCII complex is trimeric, and each monomer forms a scaffold for eight Chla and six Chlb molecules, two luteins (Lut), one neoxanthin, and one violaxanthin, which is reversibly replaced by zeaxanthin upon de-epoxidation during the xanthophyll cycle (2–4).

In addition to their light-harvesting function, LHCII complexes are involved in several regulatory mechanisms that balance the incoming excitation energies and prevent photodamage (1, 4–6). Under high sunlight conditions, the photosynthetic antenna can rapidly switch from light-harvesting into a photoprotective state in which excess light energy is safely dissipated as heat (7). This photoprotective mechanism is called non-photochemical quenching (NPQ) and protects oxygenic organisms against photooxidative damage. The major component of NPQ, *qE*, depends on the transmembrane proton gradient ΔpH. In plants, a decrease in lumenal pH triggers protonation of PsbS (8, 9) and of LHCs in photosystem II (10) and activates the conversion of the LHC-bound xanthophyll cycle carotenoid from violaxanthin to zeaxanthin (11). In green algae, PsbS is absent, and the NPQ state is triggered by LhcSR, a pigment-binding complex with a short fluorescence lifetime that senses the decrease in lumenal pH (12–14). In algae, LHCII also participates in quenching, in particular the Lhcbm1 com-

* This work was supported by the HARVEST Marie Curie Research Training Network (Grant PITN-GA-2009-238017).
[1] To whom correspondence should be addressed: Dept. of Physics, Faculty of Sciences, Vrije Universiteit, De Boelelaan 1081A, 1081 HV Amsterdam, The Netherlands. Tel.: 31-20-59-87937; E-mail: a.pandit@vu.nl.
[2] The abbreviations used are: LHC, light-harvesting complex; LHCII, light-harvesting complex II; Chl, chlorophyll; Lut, lutein; NPQ, non-photochemical quenching; MAS, magic angle spinning; CP-MAS, cross-polarization-MAS; HetCor, heteronuclear correlation; β-DM, β-dodecylmaltoside; Tricine, *N*-[2-hydroxy-1,1-bis(hydroxymethyl)ethyl]glycine; DFT, density functional theory.

ponent (15, 16). On a supramolecular scale, a reorganization of the thylakoid membrane takes place in which the LHCII complexes dissociate from photosystem II and self-associate or associate with PsbS (17–20). The supramolecular rearrangements, xanthophyll exchange, and decrease in lumenal pH were proposed to promote subtle conformational changes inside the photosystem II light-harvesting proteins, by which altered chromophore configurations create a dissipation channel for the incoming light energy (5).

To date, the molecular basis for the photophysical process of NPQ is under much debate (22–28), and it is unclear how the LHCs respond to environmental changes and energy dissipative channels are formed. The LHCII complexes of plants have been studied extensively and were shown to reversibly switch their conformation between active, unquenched and photoprotective quenched conformational states (24, 29, 30). In the photoprotective state, Chl excitations in LHCII are quenched by Chl-Lut energy transfer (24) or by low lying Chl-Lut excitonic states (23), whereas Chl-Chl charge transfer states have also been proposed (25).

There is a controversy whether the LHCII x-ray structures represent the active or quenched form of the protein (22, 31, 32). LHCII complexes reconstituted in lipid nanodiscs retained their fluorescent state but showed small spectral changes when compared with LHCII in detergent micelles (33), suggesting that the protein can adopt slightly different conformations within its active state. The quenched state is associated with a twist in the configuration of the LHCII-bound neoxanthin that may promote conformational changes at the Lut L1 site (24). Protonation of specific acidic residues under low lumenal pH conditions could trigger conformational changes of the short helix D and the BC loop (2), and these residues are important for stabilizing the complex at different pH values (34). Under NPQ conditions, changes in the thickness of the thylakoid membrane have been observed, and it was proposed that LHCII adopts a more condensed structure (35).

In this work, we applied MAS-NMR techniques in combination with selective Arg isotope labeling as a noninvasive method to obtain high-resolution structural information of LHCII in its active and photoprotective states. Photosynthetic light-harvesting proteins are accessible for NMR via uniform or selective isotope enrichment of the photosynthetic organisms (36). This way, pigment-protein interactions could be detected in atomic detail inside intact purple bacterial light-harvesting oligomers (37–39). More recently, we performed a MAS-NMR analysis of LHCII from uniformly ^{13}C-enriched *Chlamydomonas reinhardtii* green algae cells (40, 41). The *C. reinhardtii* Lhcbm sequences have a high similarity with Lhcb sequences of higher plants (40), making *C. reinhardtii* LHCII a suitable *in vitro* model system for the structural flexibility of plant Lhcb and algae Lhcbm proteins.

Here we analyze LHCII complexes from an Arg-auxotrophic strain of *C. reinhardtii* that was supplied with $^{13}C_6$-$^{15}N_4$ Arg. One-dimensional ^{13}C and ^{15}N CP-MAS and two-dimensional ^{1}H-^{13}C dipolar heteronuclear correlation (HetCor) Arg NMR spectra are presented of LHCII in quenched and unquenched states. The Arg residues that stabilize the interlocked helix pair in LHCII are identified because of Chl ring current-induced shifts of their NMR responses. We show that these protein sites are preserved in the photoprotective state, confirming a structural view in which the flexible loop regions of the LHCII polypeptides are complemented by a relatively rigid scaffolding of the protein interior (42).

EXPERIMENTAL PROCEDURES

Isotope Enrichment and Purification of LHCII Trimers—*C. reinhardtii* strain cc424, an Arg auxotrophic strain obtained commercially from the *Chlamydomonas* Connection, was grown in liquid TAP (Tris-acetate-phosphate) medium (43) with 50 mg/liter Arg used (44). Cells were cultured at room temperature under continuous illumination at 60 microeinsteins of flux. Arginine was added separately to the cell cultures, and for selective Arg enrichment, it was substituted by [$^{13}C_6$,$^{15}N_4$]Arg purchased from Silantes GmbH. The cells were harvested in mid-log phase by centrifugation (4000 rpm, 6 min, 4 °C), and thylakoids were prepared as described in Ref. 45 with a few modifications described in Ref. 46. Thylakoids were separated from other materials on a discontinuous gradient (24,000 rpm, 1 h, 4 °C) in a TST-41.14 swing-out rotor. Thylakoid membranes were washed two times, first with 10 mM HEPES, pH 7.5, and 5 mM EDTA and finally with 10 mM HEPES, pH 7.5. Thylakoids were resuspended in solubilization buffer (10 mM HEPES, pH 7.5) to a Chl concentration of 1 mg/ml, and equal amounts of β-dodecylmaltoside (β-DM) were added to get a final concentration of 0.6% β-DM. The suspension was vortexed a few seconds and centrifuged (15,000 rpm, 10 min, 4 °C) to remove unsolubilized material, and the supernatant was loaded on a sucrose density gradient, prepared by 0.65 M sucrose, 10 mM Tricine, pH 7.8, 0.03% β-DM and ultracentrifuged for 17 h at 37,000 rpm. The top band of the sucrose gradient contained LHCII trimer complexes with more than 90% purity, verified by FPLC.

For obtaining LHCII in its quenched state, isolated LHCII trimers in 0.03% β-DM were dialyzed for 72 h against detergent-free buffer. The quenched state of the detergent-depleted LHCII aggregates was verified by low temperature fluorescence spectroscopy, whereas the unquenched, light-harvesting state of the LHCII trimers in β-DM was verified by time-resolved fluorescence spectroscopy.

Fluorescence Experiments—Steady-state fluorescence excitation and emission spectra were measured with a commercial spectrophotometer (HORIBA Scientific, FluoroLog). For 77 K fluorescence emission measurements, the samples were diluted in 40% HEPES/β-DM buffer and 60% glycerol (v/v) and cooled in a nitrogen-bath cryostat to 77 K.

Time-resolved fluorescence emission measurements were performed at room temperature with a Streak camera setup. The sample was measured front-face using a 1-mm quartz cuvette. To minimize the effects of photodamage, about 10 spectra of maximum 1 min per scan were acquired. It was verified that within this time period of illumination, no degradation of sample occurred. Excitation pulses of 400 nm (~100 fs) with vertical polarization were generated using a titanium:sapphire laser (Coherent Vitesse) with a regenerative amplifier (Coherent, MIRA seed, and RegA) that was used to pump an optical parametric amplifier (Coherent, OPA). The repetition

rate was 50 kHz with pulse energies of ~0.2 nJ. A 10-fold increase or 2-fold decrease of the excitation pulse energy did not affect the fluorescence lifetimes, confirming that experiments were performed in the annihilation-free regime. The obtained streak data were analyzed with Glotaran3 (47).

Solid-state NMR Experiments—One-dimensional ^{13}C and ^{15}N and two-dimensional ^{1}H-^{13}C frequency-switched Lee-Goldburg heteronuclear correlation experiments were performed with a Bruker AV-750 spectrometer equipped with a 4-mm triple resonance MAS probe head, using a ^{13}C radio frequency of 188.6 MHz. The temperature was lowered to 220–240 K under slow spinning of the sample. For the NMR experiments, spinning frequencies of 13 kHz were used. The chemical shift scale was calibrated from an FSLG spectrum of solid tyrosine HCl salt.

Density Functional Theory Calculations—Density functional theory (DFT) calculations were performed in vacuum within the DFT framework and using the Gaussian 03 package (48). The BLYP exchange correlation function (49–51) was applied to produce the NMR chemical shifts (48, 52). The geometric arrangements of Arg-70, Glu-180, and Chl610 were extracted from the 2BHW crystallographic structure of pea LHCII (3). The phytyl group of the Chl610 was truncated at the ester group and replaced by a hydrogen atom. The truncation had no effect on the electronic structure of porphyrin ring. The geometries were partially optimized, preserving the planar structure of the Chl macrocycle and of the backbone of Arg-70 and Glu-180. The ^{1}H, ^{13}C, and ^{15}N NMR chemical shieldings were calculated by using the gauge-independent atomic orbital (54–57) on the whole complex, and subsequently, NMR calculations were performed. For both partial optimization and NMR chemical shift calculations, the BLYP/6-311G** basis set was used.

RESULTS

Fluorescence Conditions of LHCII in Detergent-solubilized and Aggregated State—LHCII was prepared in its active, light-harvesting state by solubilizing the LHCII complexes in β-DM buffer. Time-resolved fluorescence experiments on LHCII complexes concentrated in β-DM buffer solution verified that the light-harvesting state of LHCII was retained in the highly concentrated form required for the NMR experiments. Fig. 1 shows the decay-associated spectra obtained by a global analysis fitting of the streak camera images of LHCII concentrated in β-DM solution. The average fluorescence lifetime $\langle\tau_f\rangle$ of this sample is 3.0 ns and verifies that the concentrated sample of LHCII in β-DM buffer retained its unquenched state. LHCII aggregates that reflect the photoprotective state of LHCII were produced by dialysis against detergent-free buffer. For the aggregate sample, the fluorescence signal was below the detection limit of the Streak camera setup, and its quenched state was verified by a 77 K steady-state fluorescence emission spectrum. Fig. 2 presents a 77 K fluorescence spectrum of LHCII in β-DM buffer (*dashed spectrum*) and after dialysis against detergent-free buffer (*solid spectrum*). Significant fluorescence quenching of LHCII aggregates formed upon dialysis is confirmed by the 10-fold decrease and 4-nm red shift of the fluorescence peak at 675 nm and the appearance of an additional fluorescence band

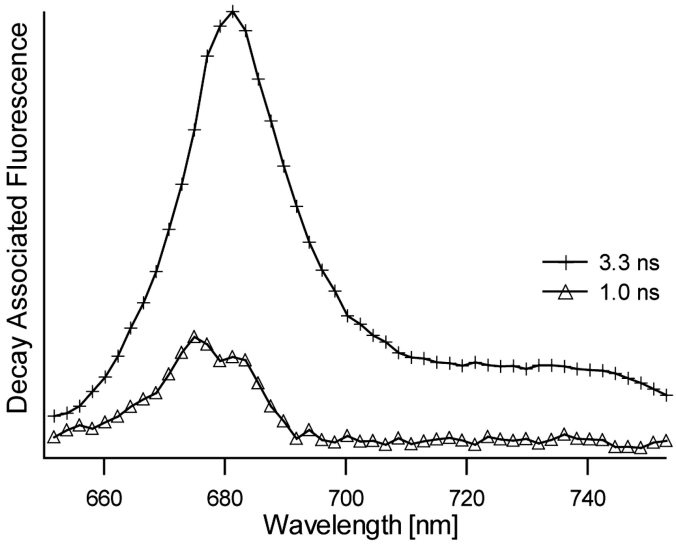

FIGURE 1. **Decay-associated fluorescence spectra and associated lifetimes of LHCII concentrated in β-DM buffer solution.**

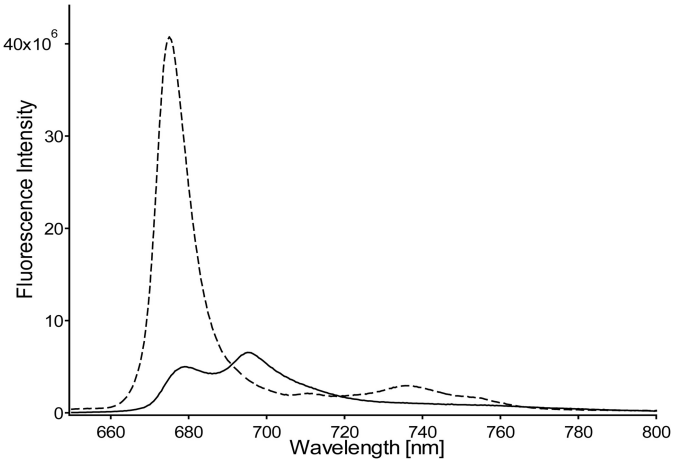

FIGURE 2. **77 K fluorescence spectra of LHCII.** *Dashed spectrum*, LHCII in β-DM buffer. *Solid spectrum*, LHCII in detergent-free buffer after extensive dialysis for removal of the β-DM.

at 695 nm, which has been associated with quenching and aggregation of LHCII (30).

Arg NMR Responses for LHCII in Its Active and Dissipative State—Fig. 3 shows the one-dimensional ^{13}C (*panel A*) and ^{15}N (*panel B*) CP-MAS spectra of quenched (*solid*) and unquenched (*dashed*) LHCII. In *panel C*, the second derivative of the ^{15}N spectra is drawn. The Arg chemical structure is drawn with the spectra in *panel A*. The natural abundance ^{13}C NMR responses of the β-DM detergent molecules is denoted with *asterisks* in the ^{13}C spectrum of unquenched LHCII. Selective [$^{13}C_6$,$^{15}N_4$]Arg enrichment of the LHCII samples is confirmed by the characteristic C_ζ Arg peaks of ~158 ppm and N_η and N_ϵ responses of ~72 and ~82 ppm, respectively. Both samples show splitting of NMR responses for the Arg C_ζ, C_δ, and C_α and for the N_η, N_ϵ, and nitrogen atoms.

Fig. 4 shows an overlay of ^{1}H-^{13}C HetCor spectra of quenched (*red*) and unquenched (*blue*) LHCII in the Arg $^{13}C_\zeta$ region (*left panel*) and $^{13}C_\delta$ region (*right panel*). The *left panel* presents the correlations between C_ζ and $H_{\eta i}/H_\epsilon$, whereas the *right panel* presents the correlations between C_δ and H_δ (pro-

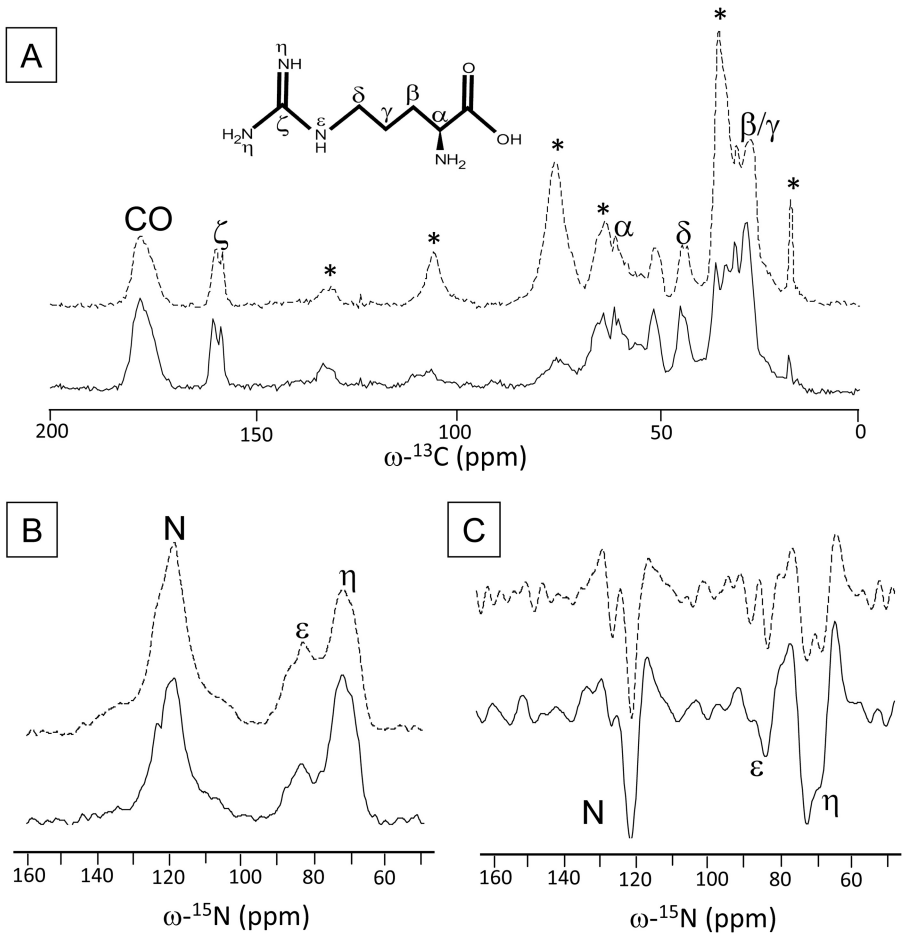

FIGURE 3. **^{13}C CP-MAS spectra of unquenched (*dashed line*) and quenched (*solid line*) LHCII.** *A*, detergent peaks in unquenched LHCII are denoted with *asterisks*. The chemical structure of Arg is also shown. *B*, ^{15}N CP-MAS spectra of unquenched (*dashed line*) and quenched (*solid line*) LHCII. *C*, second derivatives of the ^{15}N spectra in *B*.

ton range 3–5 ppm) and between C_δ and H_ϵ (proton range 6–8.5 ppm). Because the H_ϵ proton signals (*right panel*) are in the range of 6.5–8.5 ppm, the proton responses in the *left panel* between 8.5 and 10.5 ppm are attributed to the $H_{\eta i}$ protons. The *left panel* also shows very peculiar well resolved correlation signals of narrow C_ζ responses at 156.8 ppm ^{13}C associated with very upfield shifted proton responses centered around 4.2 ppm ^{1}H.

Fig. 5 shows the ^{1}H-^{13}C HetCor spectra in the region of the Arg $^{13}C_\alpha$ responses (*panel A*, unquenched LHCII, and *panel B*, quenched LHCII). The correlation signals in the range 62–64 ppm are attributed to ^{13}C natural abundance chemical shift signals of the detergent molecules. The Arg C_β and C_γ responses are strongly obscured by overlap with the detergent signals in the range 15–35 ppm and could not be resolved (data not shown). A comparison of Fig. 5, *A* and *B*, shows that the C_α correlation peak signal at 57 ppm ^{13}C and 3.2 ppm ^{1}H in the spectrum of unquenched LHCII (Fig. 5*A*) apparently shifts considerably downfield in the ^{1}H dimension and produces a doubled response for quenched LHCII (Fig. 5*B*).

DISCUSSION

The LHCII trimers of *C. reinhardtii* are isomers composed of different Lhcbm polypeptides. These Lhcbm polypeptides contain 6 Arg residues that are conserved in the Lhcb sequences of *Arabidopsis thaliana* (40). The Lhcbm1, Lhcbm5, and Lhcbm10 polypeptides contain additional Arg residues (2 residues for Lhcbm1 and 10 and 1 residues for Lhcbm5) very close to the N terminus, in a flexible part of LHCII that was not resolved in the LHCII x-ray structures. Most likely, the NMR responses of these additional Arg are also unresolved in our NMR datasets because they are only present in a subpopulation of the LHCII isomers. Moreover, their NMR responses are likely to be weakened due to intrinsic disorder of the N-terminal part, which causes dynamic broadening of the NMR lines and poor cross-polarization. For example, in MAS NMR datasets of purple bacterial antenna proteins, the terminal ends of the α- and β-polypeptides were not resolved (58).

Fig. 6*A* shows the homology structure of the *C. reinhardtii* Lhcbm1 monomer, based on the pea LHCII x-ray structure (2BHW) (3), with the 6 conserved Arg residues highlighted. Five Arg residues reside in the α-helical part of the protein, whereas the 6th Arg is located in the stromal loop region. The arginines that form ion pairs with Glu and ligate Chls, Arg-70, Arg-185, and Arg-160, are indicated in the figure, as well as Arg-25 in the loop region. Fig. 6*B* shows the arrangement of one of the stabilizing Arg-Glu pairs in detail: Arg-70 and Glu-180 that link helix A and B and ligate Chl610.

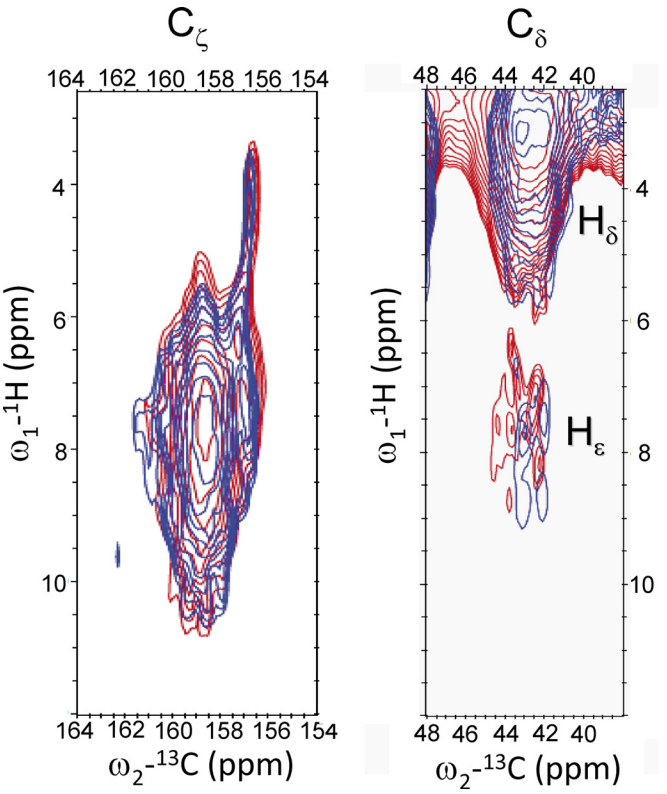

FIGURE 4. **Heteronuclear ^{1}H-^{13}C correlation spectra of unquenched (*blue*) and quenched (*red*) LHCII in the Arg $^{13}C_\zeta$ region (*left*) and in the $^{13}C_\delta$ region (*right*).**

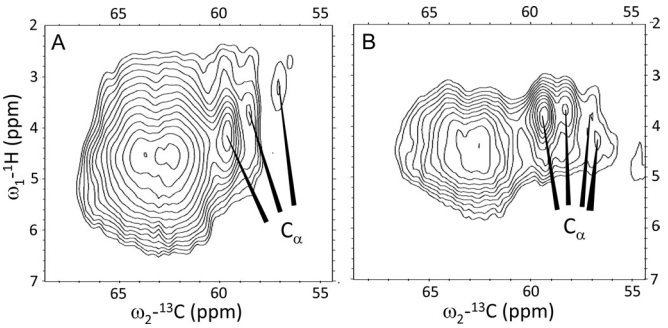

FIGURE 5. **Heteronuclear ^{1}H-^{13}C correlation spectra of unquenched (*A*) and quenched (*B*) LHCII in the Arg $^{13}C_\alpha$ region.**

According to the plant LHCII x-ray structures, the 6 Arg residues are capable of forming hydrogen bonds via their side chain H_ϵ or H_η amides. The strong downfield NMR shifts of the Arg proton responses in the HetCor spectrum in Fig. 4, *left panel*, suggest that in *C. reinhardtii* LHCII, strong hydrogen bonds are also formed to the Arg residues that involve the $NH_{\eta i}$ amide protons.

Upfield Shifted NMR Responses Are Explained by Chl Ring Current Shifts for Arg-70 and Arg-185—In the HetCor spectrum in Fig. 4, *left panel*, the $^{13}C_\zeta$ response at 156.8 ppm correlates with unusual upfield shifted proton responses at 4.2 ppm that are ~3 ppm shifted relative to the average values (7.4 and 6.8–6.9 ppm, respectively) found for Arg H_ϵ and $H_{\eta i}$ in the Biological Magnetic Resonance Bank (59). To find an explanation for these unusual shifts, we estimated the ring current effects that are produced by the Chl macrocycle rings. Chl ring currents can induce large shifts for the NMR responses of atoms in close vicinity to the ring center distances (60). Close inspection of the LHCII x-ray structures shows that both Arg-70 and Arg-185 have their side chains hanging over the macrocycle planes of the ligating Chls (Chl602 and Chl610), which positions the Arg side chain atoms close to the Chl rings. The third Arg residue involved in Chl ligation, Arg-160, forms an ion pair with a Glu residue of the same helix (helix C) and has its side chain oriented perpendicular to the macrocycle plane of its ligating Chl (Chl609). For Arg-160, only one proton is positioned close enough to the Chl ring center that it could experience significant ring current effects.

The geometric arrangements of Arg-70, Glu-180, and Chl610 as shown in Fig. 6*B* were taken from the 2BHW crystal structure and partially optimized as described under "Experimental Procedures." Quantum-mechanical DFT calculations were performed for three structure models: 1) Arg-70, 2) Arg-70···Glu-180, and 3) Arg-70···Glu-180···Chl610 to estimate the magnitude of Chl ring current and H-bonding-induced shifts of the Arg-70 NMR responses. Table 1 shows how the chemical shifts of Arg-70 (model 1) are affected by interaction with Glu-180 (model 2) and by combined interaction with Glu-180 and Chl610 (model 3). The effects of a partial geometry optimization were most critically obvious for the calculated chemical shifts of the Arg-70 H_ϵ and H_{21} atoms. For these protons also, non-optimized calculated shifts values are presented in which the geometries were taken directly from the x-ray structure.

The results in Table 1 show that for both the unmodified and the partially optimized structures, the presence of the Chl causes strong ring current shifts for the Arg-70 H_ϵ and H_{21} responses of ~−5 and ~−3.5 ppm (*i.e.* the differences between the NMR responses calculated for models 2 and 3), which we attribute primarily to the ring currents in the Chl610 that counteract the large downfield shifts due to H-bonding of these protons to the Glu-180 carboxyl. For H_ϵ, the H-bond interaction with the Glu-180 carboxyl is weakened when a ligand to magnesium is formed via the same oxygen atom, which may also affect the H_ϵ chemical shift.

The net effect of H-bonding and ring current shifts in our calculations are that the H_ϵ and H_{21} NMR responses are shifted between +3.5 and −1 ppm, depending on the optimization procedure that was applied. The net effects for the other amide protons H_{11}, H_{12}, and H_{22} are shifts between −1.5 and 2 ppm, whereas the side chain carbon responses of C_ζ and C_δ are shifted −2.7 and −2.4 ppm, respectively.

Although the exact geometries of the Arg-Glu-Chl structures may differ in *C. reinhardtii* LHCII from the plant LHCII x-ray structures, the trends of the calculated chemical shift changes match with the experimental observations of (i) C_ζ carbon responses that are shifted 2–3 ppm upfield from the bulk of C_ζ signals and that correlate with (ii) proton responses that are shifted 0–2 ppm downfield in addition to (iii) proton responses with significant upfield shifts because for the H_{11}, H_{12}, and H_{22}, the interaction with Glu-180 and Chl610 produces shifts of −1.5 to −2 ppm. Hence, according to the DFT chemical shift calculations, the upfield shifted ^{1}H-$^{13}C_\zeta$ correlations that are well resolved in Fig. 4, *left panel*, could originate from Arg-Glu-

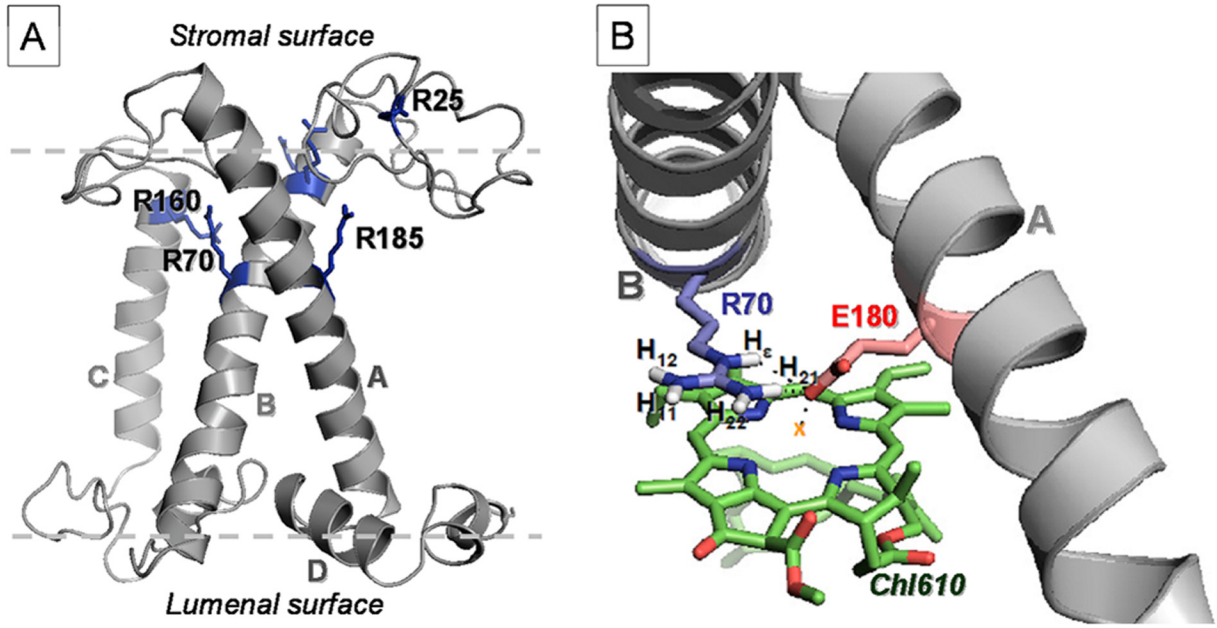

FIGURE 6. *A*, homology structure of *C. reinhardtii* LHCII highlighting the Arg residues. *B*, the geometric arrangements of Arg-70, Glu-180, and Chl610 taken from the 2BHW (3) LHCII x-ray structure.

TABLE 1

DFT-predicted NMR chemical shift displacements for Arg-70

The NMR chemical shifts of R70 were calculated using model 1 (Arg-70), model 2 (Arg-70···Glu-180), and model 3: (Arg-70···Glu-180···Chl610).

Atom	Arg-70···Glu-180 (model 2) ($\Delta\sigma$)[a]	Arg-70···Arg-180···Chl610 (model 3) ($\Delta\sigma$)[b]
	ppm	*ppm*
H_ϵ	+6.0	+1.0
H_ϵ	+3.5[c]	−1.1[c]
H_{11}	−1.1	−1.5
H_{12}	−0.9	−1.7
H_{21}	+7.0	+3.7
H_{21}	+3.0[c]	−0.6[c]
H_{22}	−0.8	−2.1
C_ζ	−1.2	−2.7
C_σ	−1.2	−2.4
N_ζ	−3.3	+1.3
N_1	+11.6	+9.5
N_2	−8.1	−6.8

[a] Chemical shift differences between model 2 and model 1.
[b] Chemical shift differences between model 3 and model 1.
[c] Non-optimized.

Chl interactions involving the two Arg residues that form an important structural motif by locking helix A and B.

Our limited models do not take into account hydrogen bonds to other parts of the protein. In the LHCII x-ray structures, one amide proton of Arg-70 is very close to the C13 keto carbonyl of Chl608. This proton is too far from the Chl ring centers to experience any ring current shift. A strong H-bond of this proton to the Chl608 carbonyl should induce a strong downfield shift of its NMR response. Instead, no strong downfield shifts are observed in the ^{1}H dimension for the C_ζ signal at 156.8 ppm. This suggests that the H-bonding patterns to the Chl side chains in *C. reinhardtii* LHCII differ from plant LHCII. In fact, in an earlier study on uniform ^{13}C-labeled *C. reinhardtii* LHCII, we estimated that the number of Chls with H-bonded keto carbonyls is lower in *C. reinhardtii* LHCII than in plant LHCII (40).

When comparing the C_ζ regions in the HetCor spectra for quenched and unquenched LHCII (Fig. 4), no significant changes are observed, and the spectra are almost identical. In particular, the unusual correlation signal with very upfield proton shifts that we attribute to the helix-connecting Arg residues is preserved. The data imply that the Arg-Glu-Chl geometric arrangements are preserved in the quenched state, relative to the unquenched state. Because the Arg-Glu pairs interlock helix A and B, the conserved chemical shift patterns suggest that the orientations of these two transmembrane helices, which define the tertiary structure, are also preserved in the two states. In addition, the Arg hydrogen-bonding patterns appear to be preserved in the two forms of LHCII.

The DFT-calculated nitrogen chemical shifts in Table 1 predict displacements of the Arg amide ^{15}N NMR responses when a hydrogen bond is formed to Glu (model 2), which breaks the symmetry of the $N_{\eta i}$ responses and induces an upfield shift of the N_ϵ response. The splitting of the Arg $^{15}N_\eta$ signal (Fig. 3, *B* and *C*) therefore can be explained by the induced asymmetry when a hydrogen bond is formed to one of the two N_η atoms, whereas splitting of the Arg N_ϵ signal is explained by heterogeneity of the Arg structures with respect to H-bonding of their side chain N_ϵ atoms.

In Quenched LHCII, Arg-25 Changes Its Backbone Conformation—The Arg $^{13}C_\alpha$ chemical shift responses reflect moderate conformational changes between the quenched and unquenched forms of LHCII. In the spectrum of unquenched LHCII, two C_α correlation signals appear at 59.5 and 58.5 ppm, and a smaller peak appears at 57 ppm. In the spectrum of quenched LHCII, the latter peak is split into two weaker signals.

The LHCII x-ray structures 2BHW (3) and 1RWT (2) were used to predict the Arg backbone chemical shifts using the SHIFTX2 server. The structure-predicted Arg C_α shifts range between 58 and 60 ppm for the residues in the α-helical stretches, whereas the Arg residue in the stromal loop region, Arg-25, has a predicted C_α shift of 56 ppm. In the NMR spectrum of unquenched LHCII (Fig. 5*A*), the relative signal intensities of the C_α peaks at 59.5, 58.5, and 57 ppm are roughly in the

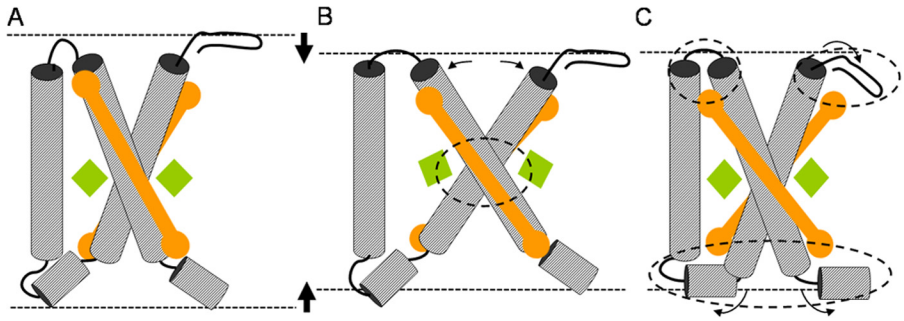

FIGURE 7. **Graphic illustrating the possible effects of membrane thinning on LHCII.** Compression of the LHC structure in *A* is achieved by (i) increased tilting of the transmembrane helices, causing structural changes in the Arg-Glu interlocked core (*B*; the affected core region is *encircled*) or (ii) reorientation of protein segments close to the water interface, causing structural changes in the regions near the lumenal and stromal sites (*C*; the affected end regions are *encircled*). A structural change as depicted in *B* will affect the orientations of Chl602 and Chl610 (*green diamonds*) that are ligated to the Arg-Glu interlocked core. However, such a structural rearrangement is unlikely according to the preserved NMR chemical shifts of the Chl-ligating Arg. The structural change depicted in *C* could reorient the luteins (*orange rods*) that have their head groups bound to the affected protein end regions.

order of 3:2:1, matching with 5 Arg residues located in the α-helical stretches that have C_α shifts in the range 58–60 ppm and one Arg residue in the loop region with a more upfield shifted C_α response. Therefore we tentatively assign the response at 57 ppm to the C_α of Arg-25 in the stromal loop region. We cannot exclude that the response at 57 ppm $^{13}C_\alpha$ includes the additional Arg residues at the N-terminal site, appearing in a subpopulation of LHCII. The backbone NMR chemical shifts of the additional Arg residues will likely fall in the chemical shift range for random coil structures, *i.e.* 54–58 ppm.

Apparently, the backbone conformation of Arg-25 (and/or of the additional Arg at the N-terminal ends) is changed in the photoprotective state (Fig. 5*B*). Arg-25 is in the water-exposed stromal region of the protein and this part of the protein is probably affected by a change in hydrophobicity or by protein-protein interactions inside the LHCII aggregates.

Stability of the Interlocked A and B Helices in the LHCII Core and Implications for Possible Conformational Changes—Early studies of Murakami and Packer (61) showed a thinning of the thylakoid membrane bilayer upon illumination together with an increase in membrane hydrophobicity, and similar effects were observed in electron microscopy micrographs of granal thylakoid membranes (17, 19). Johnson *et al.* (35) performed an extended analysis and demonstrated that apparent changes in the appressed membrane zone upon illumination correlated with structural changes in membrane thickness. The authors suggested that the observed decrease in membrane thickness reflects conformational changes of LHCII, forming a more condensed state (35). A similar condensed state is proposed to form upon aggregation *in vitro* due to protein-protein interactions and changes in hydrophobicity (5). Here we elaborate on this theory and reason that a hypothetical compressed conformation of LHCII can be established in two ways.

First, it can be established by increased helix tilting, an effect that is a common response of membrane helices to hydrophobic mismatch (53, 62). The LHCII monomers can be compressed by increasing the angles of the membrane-spanning helices A and B with respect to the membrane normal. This is illustrated in Fig. 7*B*. The LHC structure in Fig. 7*A* is compressed by increased tilting of the interlocked helices, resulting in the structure drawn in Fig. 7*B*. However, such a mechanical movement would modify the geometric arrangements of the Glu and Arg residues linking the two helices and of the Arg-Glu ligated Chls (Fig. 7*B*, *encircled area*). According to our results in Fig. 4, *left panel*, this scenario is unlikely. The NMR data show that the responses of the involved Arg residues are almost identical for the quenched and unquenched forms of LHCII, whereas our modeling results predict that these responses are very sensitive to the specific orientations of the interacting Glu, Arg, and Chls. Our findings match with the results of Dockter *et al.* (42), which show that the LHCII polypeptides have low flexibility in the core region.

Second, alternatively, a condensed state of LHCII can be created by rearrangement of protein segments located near the water interface. This is illustrated in Fig. 7*C*, where segments at the stromal and lumenal ends of the structure in Fig. 7*A* are refolded (*encircled areas*) to create a more compact conformation. Such conformational changes are in line with the NMR data and can explain the variability of the $^{13}C_\alpha$ Arg response, which we tentatively attribute to rearrangement of Arg-25 in the stromal region (Fig. 5). Although under our labeling conditions there are no residues reporting at the LHCII lumenal site, it has been proposed that changes in lumenal pH under NPQ conditions could enhance local refolding of the lumenal loop region by protonation of acidic residues (2, 34).

Photophysical quenching models have been proposed based on altered carotenoid-Chl interactions, in specific between lutein Lut620 and Chla molecules in the terminal emitter domain (Chl610, Chl611, and Chl612) (23, 24). According to our data results here on [^{13}C-^{15}N]Arg LHCII, the ring current effects of Chl610 and Chl602 acting on Arg-70 and Arg-185 do not change in the quenched state. This is a strong indication that the orientations of Chl610 and of Chl602, which are in close distance with either of the two luteins in LHCII, are preserved. The position of Chl612 is also likely to be conserved because its ligand Asn-183 is close to the Arg-Glu interlocked helical core. Thus, photophysical quenching models based on altered lutein-Chla interactions must involve a change in the orientation of a lutein chromophore with respect to the fixed positions of the adjacent Chls. Indeed, the quenched state of LHCII has been associated with a conformational change of the Lut620 carotenoid (21). A change in the orientation of a lutein could affect the NMR responses of closely spaced Chl carbons,

explaining the quenching-related changes of specific LHCII Chla NMR responses that were observed in Ref. 41. Lut620 is stabilized by protein interactions via helix D and the loop segment connecting helix A and C. In a hypothetical, mechanistic model, changes in pH and hydrophobicity may reorient these protein segments while maintaining the position of the interlocked helices A and B, resulting in a more compact protein structure as illustrated in Fig. 7*C* and moving Lut620 with respect to the fixed positions of Chl610 and Chl612, creating a photophysical quencher state.

Conclusion—We used a noninvasive method to selectively probe the structure and environment of the Arg residues in *C. reinhardtii* LHCII without the need for recombinant approaches. Our approach shows that solid-state NMR is a powerful method to determine the molecular structure of light-harvesting proteins while controlling their functional states. The conformations of the Arg residues in the α-helical regions near the stromal site and in the interlocked core are preserved in the light-harvesting and photoprotective states. In contrast, moderate changes are observed for the Arg in the stromal loop region. The results fit into a mechanistic picture where conformational changes of the LHCII end segments under NPQ conditions may reorient a carotenoid with respect to the fixed positions of the Chls in the terminal emitting domain, rendering a photophysical response for dissipation of harmful excitation energies.

Acknowledgments—Drs. Karthick Babu Sai Sankar Gupta, Fons Lefeber, and Kees Erkelens (Leiden, The Netherlands) are gratefully acknowledged for help with the solid-state NMR spectroscopy, and Dr. Francesco Buda is gratefully acknowledged for advice and discussion on the DFT calculations.

REFERENCES

1. Ballottari, M., Girardon, J., Dall'osto, L., and Bassi, R. (2012) Evolution and functional properties of photosystem II light harvesting complexes in eukaryotes. *Biochim. Biophys. Acta* **1817,** 143–157
2. Liu, Z., Yan, H., Wang, K., Kuang, T., Zhang, J., Gui, L., An, X., and Chang, W. (2004) Crystal structure of spinach major light-harvesting complex at 2.72 Ä resolution. *Nature* **428,** 287–292
3. Standfuss, J., Terwisscha van Scheltinga, A. C., Lamborghini, M., and Kühlbrandt, W. (2005) Mechanisms of photoprotection and nonphotochemical quenching in pea light-harvesting complex at 2.5 Ä resolution. *EMBO J.* **24,** 919–928
4. Barros, T., and Kühlbrandt, W. (2009) Crystallisation, structure, and function of plant light-harvesting Complex II. *Biochim. Biophys. Acta* **1787,** 753–772
5. Ruban, A. V., Johnson, M. P., and Duffy, C. D. P. (2012) The photoprotective molecular switch in the photosystem II antenna. *Biochim. Biophys. Acta* **1817,** 167–181
6. Horton, P. (2012) Optimization of light harvesting and photoprotection: molecular mechanisms and physiological consequences. *Philos. Trans. R Soc. Lond. B Biol. Sci.* **367,** 3455–3465
7. Szabó, I., Bergantino, E., and Giacometti, G. M. (2005) Light and oxygenic photosynthesis: energy dissipation as a protection mechanism against photo-oxidation. *EMBO Rep.* **6,** 629–634
8. Li, X. P., Björkman, O., Shih, C., Grossman, A. R., Rosenquist, M., Jansson, S., and Niyogi, K. K. (2000) A pigment-binding protein essential for regulation of photosynthetic light harvesting. *Nature* **403,** 391–395
9. Li, X. P., Gilmore, A. M., Caffarri, S., Bassi, R., Golan, T., Kramer, D., and Niyogi, K. K. (2004) Regulation of photosynthetic light harvesting involves intrathylakoid lumen pH sensing by the PsbS protein. *J. Biol. Chem.* **279,** 22866–22874
10. Walters, R. G., Ruban, A. V., and Horton, P. (1996) Identification of proton-active residues in a higher plant light-harvesting complex. *Proc. Natl. Acad. Sci. U.S.A.* **93,** 14204–14209
11. Müller, P., Li, X. P., and Niyogi, K. K. (2001) Non-photochemical quenching. A response to excess light energy. *Plant Physiol.* **125,** 1558–1566
12. Bonente, G., Ballottari, M., Truong, T. B., Morosinotto, T., Ahn, T. K., Fleming, G. R., Niyogi, K. K., and Bassi, R. (2011) Analysis of LhcSR3, a protein essential for feedback de-excitation in the green alga *Chlamydomonas reinhardtii*. *PLoS Biol.* **9,** e1000577
13. Bonente, G., Passarini, F., Cazzaniga, S., Mancone, C., Buia, M. C., Tripodi, M., Bassi, R., and Caffarri, S. (2008) The occurrence of the *psbS* gene product in *Chlamydomonas reinhardtii* and in other photosynthetic organisms and its correlation with energy quenching. *Photochem. Photobiol.* **84,** 1359–1370
14. Peers, G., Truong, T. B., Ostendorf, E., Busch, A., Elrad, D., Grossman, A. R., Hippler, M., and Niyogi, K. K. (2009) An ancient light-harvesting protein is critical for the regulation of algal photosynthesis. *Nature* **462,** 518–521
15. Elrad, D., Niyogi, K. K., and Grossman, A. R. (2002) A major light-harvesting polypeptide of photosystem II functions in thermal dissipation. *Plant Cell* **14,** 1801–1816
16. Ferrante, P., Ballottari, M., Bonente, G., Giuliano, G., and Bassi, R. (2012) LHCBM1 and LHCBM2/7 polypeptides, components of major LHCII complex, have distinct functional roles in photosynthetic antenna system of *Chlamydomonas reinhardtii*. *J. Biol. Chem.* **287,** 16276–16288
17. Johnson, M. P., Goral, T. K., Duffy, C. D. P., Brain, A. P. R., Mullineaux, C. W., and Ruban, A. V. (2011) Photoprotective energy dissipation involves the reorganization of photosystem II light-harvesting complexes in the grana membranes of spinach chloroplasts. *Plant Cell* **23,** 1468–1479
18. Goral, T. K., Johnson, M. P., Brain, A. P. R., Kirchhoff, H., Ruban, A. V., and Mullineaux, C. W. (2010) Visualizing the mobility and distribution of chlorophyll proteins in higher plant thylakoid membranes: effects of photoinhibition and protein phosphorylation. *Plant J.* **62,** 948–959
19. Kirchhoff, H., Hall, C., Wood, M., Herbstová, M., Tsabari, O., Nevo, R., Charuvi, D., Shimoni, E., and Reich, Z. (2011) Dynamic control of protein diffusion within the granal thylakoid lumen. *Proc. Natl. Acad. Sci. U.S.A.* **108,** 20248–20253
20. Betterle, N., Ballottari, M., Zorzan, S., de Bianchi, S., Cazzaniga, S., Dall'osto, L., Morosinotto, T., and Bassi, R. (2009) Light-induced dissociation of an antenna hetero-oligomer is needed for non-photochemical quenching induction. *J. Biol. Chem.* **284,** 15255–15266
21. Ilioaia, C., Johnson, M. P., Liao, P. N., Pascal, A. A., van Grondelle, R., Walla, P. J., Ruban, A. V., and Robert, B. (2011) Photoprotection in plants involves a change in lutein 1 binding domain in the major light-harvesting complex of photosystem II. *J. Biol. Chem.* **286,** 27247–27254
22. Barros, T., Royant, A., Standfuss, J., Dreuw, A., and Kühlbrandt, W. (2009) Crystal structure of plant light-harvesting complex shows the active, energy-transmitting state. *EMBO J.* **28,** 298–306
23. Bode, S., Quentmeier, C. C., Liao, P. N., Hafi, N., Barros, T., Wilk, L., Bittner, F., and Walla, P. J. (2009) On the regulation of photosynthesis by excitonic interactions between carotenoids and chlorophylls. *Proc. Natl. Acad. Sci. U.S.A.* **106,** 12311–12316
24. Ruban, A. V., Berera, R., Ilioaia, C., van Stokkum, I. H. M., Kennis, J. T. M., Pascal, A. A., van Amerongen, H., Robert, B., Horton, P., and van Grondelle, R. (2007) Identification of a mechanism of photoprotective energy dissipation in higher plants. *Nature* **450,** 575–578
25. Miloslavina, Y., Wehner, A., Lambrev, P. H., Wientjes, E., Reus, M., Garab, G., Croce, R., and Holzwarth, A. R. (2008) Far-red fluorescence: a direct spectroscopic marker for LHCII oligomer formation in non-photochemical quenching. *FEBS Lett.* **582,** 3625–3631
26. Liao, P. N., Pillai, S., Kloz, M., Gust, D., Moore, A. L., Moore, T. A., Kennis, J. T. M., van Grondelle, R., and Walla, P. J. (2012) On the role of excitonic interactions in carotenoid-phthalocyanine dyads and implications for photosynthetic regulation. *Photosynth. Res.* **111,** 237–243
27. Berera, R., Herrero, C., van Stokkum, I. H. M., Vengris, M., Kodis, G., Palacios, R. E., van Amerongen, H., van Grondelle, R., Gust, D., Moore,

T. A., Moore, A. L., and Kennis, J. T. M. (2006) A simple artificial light-harvesting dyad as a model for excess energy dissipation in oxygenic photosynthesis. *Proc. Natl. Acad. Sci. U.S.A.* **103,** 5343–5348
28. Holt, N. E., Zigmantas, D., Valkunas, L., Li, X. P., Niyogi, K. K., and Fleming, G. R. (2005) Carotenoid cation formation and the regulation of photosynthetic light harvesting. *Science* **307,** 433–436
29. Krüger, T. P. J., Novoderezhkin, V. I., Ilioaia, C., and van Grondelle, R. (2010) Fluorescence spectral dynamics of single LHCII trimers. *Biophys. J.* **98,** 3093–3101
30. Ruban, A. V., and Horton, P. (1992) Mechanism of ΔpH-dependent dissipation of absorbed excitation-energy by photosynthetic membranes. 1. Spectroscopic analysis of isolated light-harvesting complexes. *Biochim. Biophys. Acta* **1102,** 30–38
31. Pascal, A. A., Liu, Z., Broess, K., van Oort, B., van Amerongen, H., Wang, C., Horton, P., Robert, B., Chang, W., and Ruban, A. (2005) Molecular basis of photoprotection and control of photosynthetic light-harvesting. *Nature* **436,** 134–137
32. van Oort, B., Maréchal, A., Ruban, A. V., Robert, B., Pascal, A. A., de Ruijter, N. C. A., van Grondelle, R., and van Amerongen, H. (2011) Different crystal morphologies lead to slightly different conformations of light-harvesting complex II as monitored by variations of the intrinsic fluorescence lifetime. *Phys. Chem. Chem. Phys.* **13,** 12614–12622
33. Pandit, A., Shirzad-Wasei, N., Wlodarczyk, L. M., van Roon, H., Boekema, E. J., Dekker, J. P., and de Grip, W. J. (2011) Assembly of the major light-harvesting complex II in lipid nanodiscs. *Biophys. J.* **101,** 2507–2515
34. Yang, C., Lambrev, P., Chen, Z., Jávorfi, T., Kiss, A. Z., Paulsen, H., and Garab, G. (2008) The negatively charged amino acids in the lumenal loop influence the pigment binding and conformation of the major light-harvesting chlorophyll a/b complex of photosystem II. *Biochim. Biophys. Acta* **1777,** 1463–1470
35. Johnson, M. P., Brain, A. P. R., and Ruban, A. V. (2011) Changes in thylakoid membrane thickness associated with the reorganization of photosystem II light harvesting complexes during photoprotective energy dissipation. *Plant Signal. Behav.* **6,** 1386–1390
36. Pandit, A., and de Groot, H. J. M. (2012) Solid-state NMR applied to photosynthetic light-harvesting complexes. *Photosynth. Res.* **111,** 219–226
37. Pandit, A., Buda, F., van Gammeren, A. J., Ganapathy, S., and de Groot, H. J. M. (2010) Selective chemical shift assignment of bacteriochlorophyll a in uniformly [^{13}C-^{15}N]-labeled light-harvesting 1 complexes by solid-state NMR in ultrahigh magnetic field. *J. Phys. Chem. B* **114,** 6207–6215
38. Pandit, A., Wawrzyniak, P. K., van Gammeren, A. J., Buda, F., Ganapathy, S., and de Groot, H. J. M. (2010) Nuclear magnetic resonance secondary shifts of a light-harvesting 2 complex reveal local backbone perturbations induced by its higher-order interactions. *Biochemistry* **49,** 478–486
39. van Gammeren, A. J., Buda, F., Hulsbergen, F. B., Kiihne, S., Hollander, J. G., Egorova-Zachernyuk, T. A., Fraser, N. J., Cogdell, R. J., and de Groot, H. J. M. (2005) Selective chemical shift assignment of B800 and B850 bacteriochlorophylls in uniformly [^{13}C,^{15}N]-labeled light-harvesting complexes by solid-state NMR spectroscopy at ultra-high magnetic field. *J. Am. Chem. Soc.* **127,** 3213–3219
40. Pandit, A., Morosinotto, T., Reus, M., Holzwarth, A. R., Bassi, R., and de Groot, H. J. M. (2011) First solid-state NMR analysis of uniformly ^{13}C-enriched major light-harvesting complexes from *Chlamydomonas reinhardtii* and identification of protein and cofactor spin clusters. *Biochim. Biophys. Acta* **1807,** 437–443
41. Pandit, A., Reus, M., Morosinotto, T., Bassi, R., Holzwarth, A. R., and De Groot, H. J. M. (2013) An NMR comparison of the light-harvesting complex II (LHCII) in active and photoprotective states reveals subtle changes in the chlorophyll a ground-state electronic structures. *Biochim. Biophys. Acta* **1827,** 738–744
42. Dockter, C., Müller, A. H., Dietz, C., Volkov, A., Polyhach, Y., Jeschke, G., and Paulsen, H. (2012) Rigid core and flexible terminus: structure of solubilized light-harvesting chlorophyll a/b complex (LHCII) measured by EPR. *J. Biol. Chem.* **287,** 2915–2925
43. Gorman, D. S., and Levine, R. P. (1965) Cytochrome f and plastocyanin: their sequence in the photosynthetic electron transport chain of *Chlamydomonas reinhardtii*. *Proc. Natl. Acad. Sci. U.S.A.* **54,** 1665–1669
44. Naumann, B., Stauber, E. J., Busch, A., Sommer, F., and Hippler, M. (2005) N-terminal processing of Lhca3 is a key step in remodeling of the photosystem I-light-harvesting complex under iron deficiency in *Chlamydomonas reinhardtii*. *J. Biol. Chem.* **280,** 20431–20441
45. Drop, B., Webber-Birungi, M., Fusetti, F., Kouřil, R., Redding, K. E., Boekema, E. J., and Croce, R. (2011) Photosystem I of *Chlamydomonas reinhardtii* contains nine light-harvesting complexes (Lhca) located on one side of the core. *J. Biol. Chem.* **286,** 44878–44887
46. Germano, M., Yakushevska, A. E., Keegstra, W., van Gorkom, H. J., Dekker, J. P., and Boekema, E. J. (2002) Supramolecular organization of photosystem I and light-harvesting complex I in *Chlamydomonas reinhardtii*. *FEBS Lett.* **525,** 121–125
47. Snellenburg, J. J., Laptenok, S. P., Seger, R., Mullen, K. M., and van Stokkum, I. H. M. (2012) Glotaran: A Java-based graphical user interface for the R package TIMP. *J. Stat. Softw.* **49,** 1–22
48. Wawrzyniak, P. K., Alia, A., Schaap, R. G., Heemskerk, M. M., de Groot, H. J. M., and Buda, F. (2008) Protein-induced geometric constraints and charge transfer in bacteriochlorophyll-histidine complexes in LH2. *Phys. Chem. Chem. Phys.* **10,** 6971–6978
49. Becke, A. D. (1988) Density-functional exchange-energy approximation with correct asymptotic behavior. *Phys. Rev. A* **38,** 3098–3100
50. Miehlich, B., Savin, A., Stoll, H., and Preuss, H. (1989) Results obtained with the correlation energy density functionals of Becke and Lee, Yang and Parr. *Chem. Phys. Lett.* **157**, 200–206
51. Lee, C., Yang, W., and Parr, R. G. (1988) Development of the Colle-Salvetti correlation-energy formula into a functional of the electron density. *Phys. Rev. B Condens. Matter* **37**, 785–789
52. Facelli, J. C. (1998) Density functional theory calculations of the structure and the ^{15}N and ^{13}C chemical shifts of methyl bacteriopheophorbide a and bacteriochlorophyll a. *J. Phys. Chem. B* **102**, 2111–2116
53. Kim, T., and Im, W. (2010) Revisiting hydrophobic mismatch with free energy simulation studies of transmembrane helix tilt and rotation. *Biophys. J.* **99,** 175–183
54. Ditchfield, R. (1981) Theoretical studies of the temperature dependence of magnetic shielding tensors: H_2, HF, and LiH. *Chem. Phys.* **63,** 185–202
55. Wolinski, K., Hinton, J. F., and Pulay, P. (1990) Efficient implementation of the gauge-independent atomic orbital method for NMR chemical shift calculations. *J. Am. Chem. Soc.* **112**, 8251–8260
56. McWeeny, R. (1962) Perturbation theory for the Fock-Dirac density matrix. *Phys. Rev.* **126**, 1028–1034
57. Woliński, K., and Sadlej, A. J. (1980) Self-consistent perturbation theory: Open-shell states in perturbation-dependent non-orthogonal basis sets. *Mol. Phys.* **41,** 1419–1430
58. van Gammeren, A. J., Hulsbergen, F. B., Hollander, J. G., and de Groot, H. J. M. (2005) Residual backbone and side-chain ^{13}C and ^{15}N resonance assignments of the intrinsic transmembrane light-harvesting 2 protein complex by solid-state Magic Angle Spinning NMR spectroscopy. *J. Biomol. NMR* **31,** 279–293
59. Ulrich, E. L., Akutsu, H., Doreleijers, J. F., Harano, Y., Ioannidis, Y. E., Lin, J., Livny, M., Mading, S., Maziuk, D., Miller, Z., Nakatani, E., Schulte, C. F., Tolmie, D. E., Kent Wenger, R., Yao, H., and Markley, J. L. (2008) BioMagResBank. *Nucleic Acids Res.* **36,** D402–D408
60. Abraham, R. J., and Smith, K. M. (1983) NMR spectra of porphyrins. 21. Applications of the ring-current model to porphyrin and chlorophyll aggregation. *J. Am. Chem. Soc.* **105,** 5734–5741
61. Murakami, S., and Packer, L. (1970) Protonation and chloroplast membrane structure. *J. Cell Biol.* **47,** 332–351
62. Park, S. H., and Opella, S. J. (2005) Tilt angle of a trans-membrane helix is determined by hydrophobic mismatch. *J. Mol. Biol.* **350,** 310–318

Insights into the Photoprotective Switch of the Major Light-harvesting Complex II (LHCII): A PRESERVED CORE OF ARGININE-GLUTAMATE INTERLOCKED HELICES COMPLEMENTED BY ADJUSTABLE LOOPS

Kiran Sunku, Huub. J. M. de Groot and Anjali Pandit

J. Biol. Chem. 2013, 288:19796-19804.
doi: 10.1074/jbc.M113.456111 originally published online April 29, 2013
